Science of the Total Environment 766 (2021) 142517

Contents lists available at ScienceDirect

Science of the Total Environment

journal homepage: www.elsevier.com/locate/scitotenv

Gravel replenishment and active-channel widening for braided-river restoration: The case of the Upper Drac River (France)

Guillaume Brousse [a,*], Frédéric Liébault [b], Gilles Arnaud-Fassetta [a], Bertrand Breilh [c], Sandrine Tacon [d]

[a] Université de Paris (Diderot), UMR 8586 (PRODIG), Paris, France
[b] Université Grenoble Alpes, INRAE, ETNA, Grenoble, France
[c] CLEDA, Saint-Bonnet-en-Champsaur, France
[d] Morph'eau Conseils, Chazay d'Azergues, France

HIGHLIGHTS

- Physical effects of the restoration of a degraded braided river in the French Alps
- Topographic differencing, bedload tracing and historical channel changes
- A spontaneous braiding recovery after replenishment and channel widening
- Braiding conditions in the near future remain uncertain.

GRAPHICAL ABSTRACT

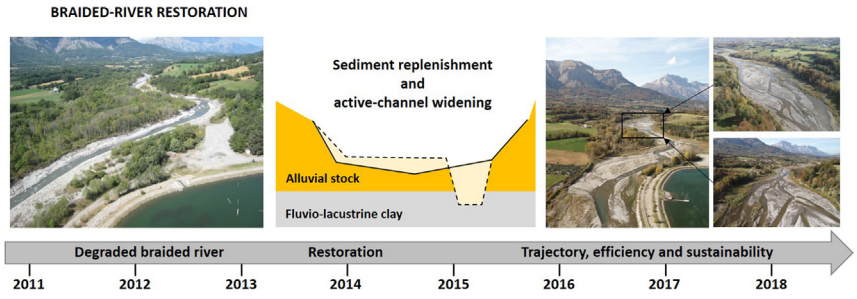

ARTICLE INFO

Article history:
Received 3 July 2020
Received in revised form 14 September 2020
Accepted 16 September 2020
Available online 2 October 2020

Editor: Fernando A.L. Pacheco

Keywords:
Braided river
Hydromorphological restoration
Gravel replenishment

ABSTRACT

Massive gravel replenishment combined with active-channel widening could theoretically improve the morphological recovery of altered braided rivers but this restoration strategy was not yet tested in the field. A recent braided restoration project based on this principle was set up to restore a 4.2 km long reach in the Upper Drac River (French Alps) using 355.000 m^3 of gravels to rise the bed level and to design a 100-m wide trapezoidal cross-section. The aim of this paper is to capture the morphological trajectory after restoration in order to evaluate efficiency and sustainability of this strategy. A Before and After Control Impact monitoring design has been used by combining a repetitive topographic survey (using airborne LiDAR data and terrestrial topographic surveys along cross-sections), an assessment of bedload supply to the restored reach using sediment tracing and active-layer surveys, and a systematic analysis of historical aerial photographs. In a particular context of low hydrological forcing after restoration, the restored reach adjusts with local braiding reference that highlights the efficiency of the restoration strategy. Despite this spontaneous braiding recovery, scouring processes are observed locally along the restored reach and the sustainability remains uncertain even if a good connection to sediment sources was observed. Feedbacks make it possible to propose recommendations to river managers who plan to use similar strategy of braided river restoration. This field study demonstrated for the first time that sediment replenishment combined with channel widening can be an efficient solution for the spontaneous recovery of braiding conditions in altered alpine gravel-bed rivers.

1. Introduction

Braided rivers are typical, fluvial forms associated with a high sediment supply, and a subsequent transport-limited morphological regime (Schumm, 1981; Ashmore, 2013). These conditions explain the formation of wide active channels composed of a complex assemblage of bars, which can be more or less vegetated, and which are separated by a network of instable low-flow channels, sometimes referred as anabranches (Nanson and Knighton, 1996; Piégay et al., 2009). This multi-thread channel pattern is emblematic of fluvial environments draining mountainous catchments with high sediment production.

* Corresponding author.
E-mail address: guillaume.brousse@enpc.fr (G. Brousse).

https://doi.org/10.1016/j.scitotenv.2020.142517
0048-9697/

Braiding was more frequent in Europe during the Little Ice Age (16th to 19th century), but starts to decline since the early 20th century in relation with a global decrease of sediment supply from catchments (e.g., Bravard and Peiry, 1993; Surian and Rinaldi, 2003; Liébault et al., 2013). This climate-driven change of erosion conditions has been strongly amplified by (i) spontaneous reforestation following rural depopulation since the 1950s, and (ii) torrent-control works during the 1860–1915 period (e.g., Liébault and Piégay, 2002; Liébault et al., 2005; Astrade et al., 2011), as well as (iii) local human pressures on sediment transport continuity (gravel mining in active channels, river regulation and dam construction). As a consequence, strong bed incision and active-channel narrowing are observed in many braided rivers. A general decrease of braiding activity is observed, which can lead to 'fluvial metamorphosis' (sustainable shift from a multi-thread to a single-thread pattern, sensu Schumm, 1981). These adjustments have a direct impact on infrastructures like bridges, dikes, or roads, and induce a dramatic loss of aquatic habitats (e.g., Bravard et al., 1997; Belletti et al., 2013; Marmonier et al., 2019).

The very active morphodynamics of braided rivers is at the origin of complex mosaics of aquatic and terrestrial habitats, which have been described as reference ecosystems for the Alps (Ward et al., 1999). This spatial heterogeneity of habitats is supporting a rich freshwater biodiversity including emblematic endangered fish or plant species in Europe, like Rhône zingel (*Zingel asper*), dwarf bulrush (*Typha minima*), or German tamarisk (*Myricaria germanica*). It is also recognized that braided rivers are a natural heritage at risk in the European Alpine environments, due to increasing human pressures on floodplains, and that it is crucial to preserve or restore rivers and floodplain corridors that are still dynamic (Le Lay et al., 2013; Ioana-Toroimac et al., 2017; Muhar et al., 2019). This is also true for New Zealand where ecological restoration of an altered braided river has been reported (Caruso, 2006).

The restoration of braided rivers generally involves localized and punctual actions (in space and time) for recovering transport-limited sediment regimes. The most common restoration actions consist to increase the sediment supply of braided rivers by dikes or dam removal (Piégay et al., 2006; Habersack and Piégay, 2007; Terrier et al., 2019). At a smaller scale, vegetation clearing in active channels has been tested to increase the remobilization of gravel bars (e.g., Hicks et al., 2009). In all cases, strategies are based on a gradual (midterm to long term) braided pattern recovery driven by floods and associated bedload transport processes that have been reactivated. Success of these restoration works depends on three conditions: (i) a sufficiently high sediment supply to maintain the braided pattern over time, implying good conditions of sediment continuity between the restored reach and its main sediment sources; (ii) an active flood regime for the regular morphological resetting of the active channel (through channel shifting and associated bar creation and destruction); and (iii) a low lateral confinement of the active channel to make sure that enough space is available in the floodplain for the development of the braided pattern. In many environmental settings, these three conditions are not satisfied and the recreation of braided riverscapes seems not to be a good option for improving the hydromorphological status of rivers (Wyzga et al., 2016).

Gravel augmentation or replenishment means artificially adding gravels in a river channel. It is generally applied to compensate sediment deficit below dams (Bunte, 2004; Sumi, 2006; Kondolf et al., 2014; Brousse et al., 2020) and it is theoretically a potential way for reactivating braiding processes in river channels impacted by a sediment-supply decrease (Staentzel et al., 2020). When such operations are combined with channel widening, they can be very efficient for the spontaneous recreation of braided channels. We know braiding is forming when runoff with a high bedload concentration is spreading in wide and gentle-slope valley settings. Many incised Alpine rivers are draining catchments where present-day catchment-scale conditions of sediment supply can be considered as favorable to braiding (Liébault et al., 2013). The incision of these rivers is generally related to strong human pressures on sediment transport at the reach-scale, like gravel mining or dam construction. In such context, the spontaneous braiding recovery should be possible after eliminating or decreasing local pressures on sediment transport. The morphological recovery may also be accelerated by artificial gravel replenishment and widening, but this needs to be tested with well-designed field experiments, which are still missing.

An emblematic restoration project including massive gravel augmentation and channel widening was recently implemented in the Upper Drac River (French Alps) to stop an accelerated channel incision and recreate a braided channel along a highly altered single-thread reach (Laval and Guilmin, 2014). This field experiment is likely the largest ever done in Alpine rivers in terms of braided-pattern restoration, and it provides a unique opportunity to investigate the channel response to a very ambitious operation of gravel replenishment and channel widening. The main goal of this study is to investigate the morphological trajectory (2014–2018) of the restored reach of the Upper Drac River using an intensive field-based monitoring approach. The scientific objectives are: (i) to determine if the restoration project has been able to stop the accelerated channel incision and to spontaneously recreate a braided channel along the restored reach; (ii) to compare the morphological signature of the recreated braided pattern with the most-preserved braided section in the catchment; and to (iii) evaluate if the recreated braided channel along the restored reach will persist in the near future, notably by looking at sediment connectivity with its main proximal sediment source.

In the first part, the study site and the restoration project are presented. In the second part, the methodological procedures for field data acquisition and processing are described. In the third part results are presented including the historical braiding evolution, the evaluation of the bedload supply to the restored reach, the topographic differencing and the morphological trajectory following restoration. Finally, discussion focuses on the reliability of the sediment balance derived from sequential LiDAR data, the efficiency of the restoration works to stop channel incision and recreate a braided channel, and the sustainability of the braided pattern recovery.

2. The study site

2.1. General presentation

The Drac River, a gravel-bed, braided river of the French Alps, is a major Alpine tributary (Strahler's rank 6) of the Isère River (rank 7 at the confluence at Grenoble; Fig. 1). The study reach is located in the Champsaur valley and extend from Saint-Jean-Saint-Nicolas to Saint-Bonnet-en-Champsaur (14.1 km). This reach drains a 340-km^2 upland catchment with a maximum elevation of 3441 m. Metamorphic rocks (mainly gneiss) are located in the upper catchment of the Drac Blanc River; the rest of the catchment is underlain by sedimentary rocks from Jurassic (black marls) to Cretaceous (limestones) and Cenozoic (sandstones) ages. Imprints from the Pleistocene are widespread in the catchment with important till deposits on hillslopes. Of particular importance is the presence of lacustrine deposits (thickness > 40 m) in the valley floor, related to the obstruction of the valley by the Séveraisse Glacier during Würmian phases of glacier recession (Montjuvent, 1978). These clay deposits are covered by the thin (thickness < 5 m) contemporary alluvial fill of the Drac River. The climate is characterized by a mean annual rainfall of ~950 mm. The hydrological regime is influenced by a strong spring snowmelt. Sediment supply is important in the upper catchment, which is yielded by active debris-flow torrents of the Drac Blanc and Drac Noir subcatchments, but not in the Champsaur valley where just few torrents are active (Torrent d'Ancelle and Brutinel on the left bank of the Upper Drac River).

Three different homogeneous hydromorphological units (HUMs) are identified along the study reach, from upstream to downstream (Fig. 1; Table A.1). HUM1 corresponds to the well-preserved braided corridor of the Chabottes plain. HUM2 corresponds to a wandering reach laterally confined by hillslopes, located downstream of the alluvial fans of the

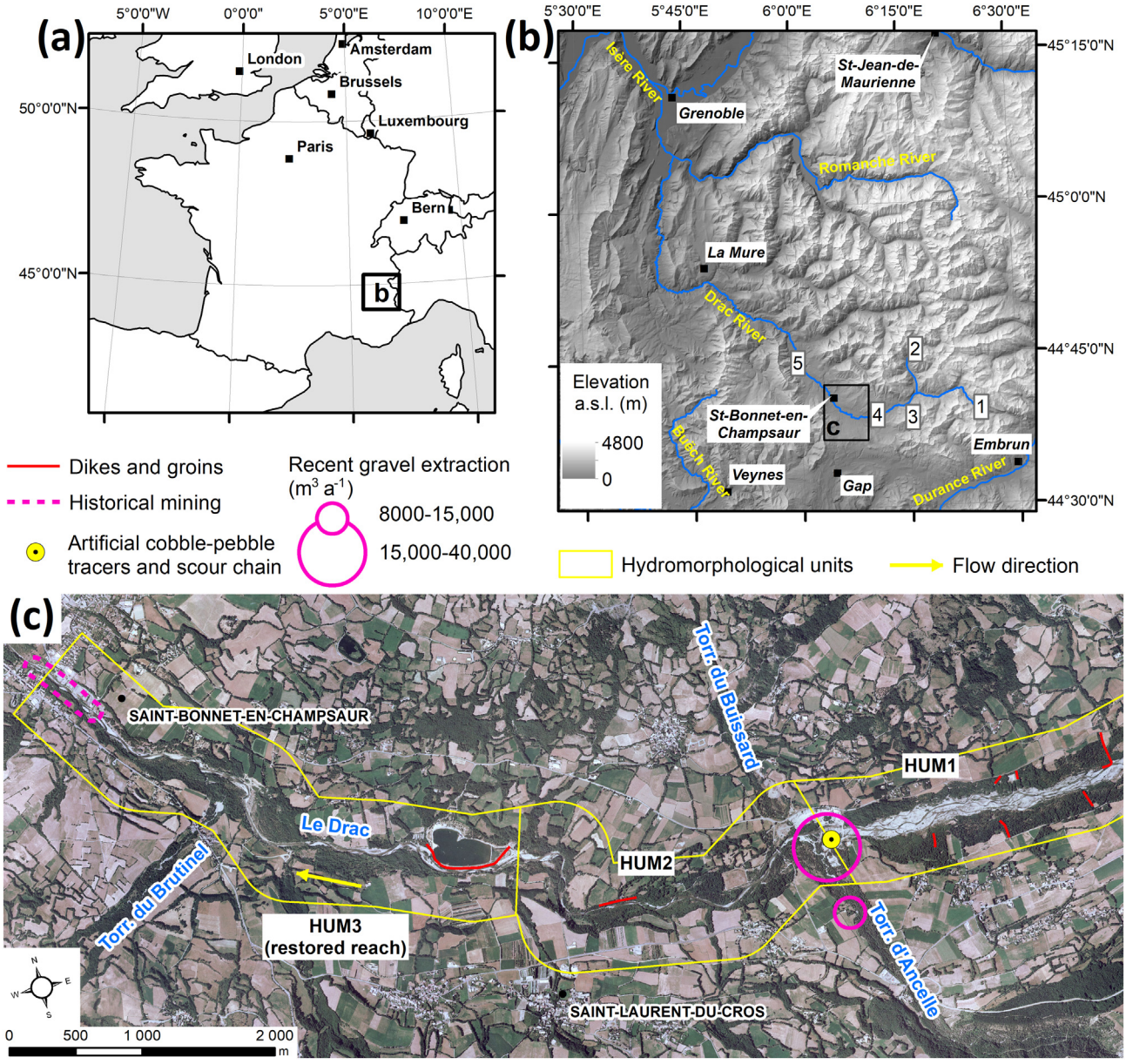

Fig. 1. General presentation of the Upper Drac River; (a) Location of the Drac catchment in France; (b) Location of the study reach in the Drac catchment (1: Drac Noir River; 2: Drac Blanc River; 3: Ricous gauging station; 4: Chabottes gauging station; 5: Guinguette gauging station); (c) Detailed map of the study reach, showing the three homogeneous hydromorphological units (human pressure is from CLEDA observatory and orthophoto dates from 2003).

Torrent d'Ancelle and of the Torrent du Buissard. HUM3 corresponds to the restored reach in which human activities are more present due to the Champsaur leisure center (artificial lake for recreational purposes) constructed in the 1990s. This touristic infrastructure is protected from high flows by a longitudinal dike, which has shallow foundations.

2.2. Why and how restoring the braided pattern of the Upper Drac River?

The Upper Drac River has been highly impacted by intensive gravel mining since the late 1960s (ETRM, 2010). This activity ceased only very recently (in 2012 according to CLEDA, the local authority in charge of water management in the Upper Drac River). Official gravel mining sites were concentrated in the Drac Blanc River (55,000 m^3 a^1) and Drac Noir River (8000 m^3 a^{-1}) subcatchments, and at the confluence with the Ancelle torrent (15,000 m^3 a^{-1}). Another mining site was active during the 1970s and 1980s downstream of the Saint-Bonnet-en-Champsaur bridge. Administrative authorizations show that the total rate of gravel mining in the Upper Drac River may have reached 93,000 m^3 a^{-1}, representing 93% of the mean annual bedload yield estimated from gravel deposition in the deltaic plain of the Sautet reservoir, located at the mouth of the Champsaur valley (Vivian and Thomas, 1982).

In addition to gravel mining, the sediment supply from lateral channel shifting has been reduced by flood and bank protection works. Most of the embankments and groynes were constructed at the beginning of the 19th century (CLEDA, 2010). Along the study reach, 19% of the bank network can be considered as controlled by protection structures. Only two major grade-control weirs are present upstream of the study reach: the *Seuil des Ricous* (4-m high) and the *Seuil de Saint-Jean-Saint-Nicolas* (1-m high), which were partially erased in 2014 and 2003, respectively.

These human alterations of the sediment regime resulted in important channel responses, like active-channel narrowing, and channel degradation, as attested by the historical long profile of 1913 (Liébault et al., 2013). A shift from a braided to a wandering pattern can be clearly observed in HUM3. Near Saint-Bonnet-en-Champsaur, the incision reaches 2 to 4 m deep, and propagates upstream (Laval and Guilmin, 2014; Fig. 2a). This incision rapidly cut through the relatively thin

alluvial layer, and starts to scour fluvio-lacustrine clay deposits from the late Pleistocene. Once this clay layer has been reached, the incision dramatically accelerates, and a 4 to 5 m deep canyon-like channel formed along the Upper Drac River (Fig. 2b and c). This dramatic accelerated channel incision has several consequences: (i) destabilization of the river banks, with a direct threat for the artificial pond of the Champsaur leisure center; (ii) lowering of the water table and subsequent alteration of the riparian forest; (iii) alteration of aquatic habitats related to the loss of gravel substrate and to the expanding clay outcrops.

The restoration project of the degraded reach near Saint-Bonnet-en-Champsaur was implemented between November 2013 and April 2014 and consisted in the creation of a new wide and shallow channel (Fig. 2d) using more than 355,000 m^3 of coarse sediment from adjacent alluvial terraces (307,000 m^3) and other complementary sources (48,000 m^3). This is an operation of channel widening using a designed 100-m wide trapezoidal cross-section, associated with a general rise of the riverbed-level. One pre-existing weir located downstream of the restored reach was raised to control the base level of the replenished reach, and equipped with fish passes. This restoration project is based on the principle of a spontaneous recovery of the braiding pattern, after having widened and raised the active channel with coarse sediment. This restoration strategy was also designed to improve the strong morphological alteration of the reach located downstream HUM3.

3. Material and methods

The physical monitoring (Fig. A.2) combines (i) a bedload tracing program using active ultra-high frequency radio-frequency identification (aUHF-RFID) technology, associated with a monitoring of the active layer (scour-and-fill processes); (ii) repetitive high-resolution topographic surveys of the study reach using airborne LiDAR data, completed with terrestrial topographic surveys along cross-sections; and (iii) a systematic analysis of historical aerial photographs. According to the comprehensive classification of restoration monitoring designs presented in Roni et al. (2013), the physical monitoring strategy of the Upper Drac River can be classified as a BACI (Before and After Control Impact) design, since pre-restoration data are generally available, and since a control site is generally used to evaluate the restoration effects. However, this has not been possible for every investigated parameters. HUM1 has been considered as the reference site; it corresponds to the Chabottes plain, a well-preserved braided-river reach located upstream of the restored reach.

3.1. Bedload tracing program

A bedload tracing program was implemented in January 2017 to evaluate the sediment connectivity between HUM1 and HUM3. Artificial cobbles and pebbles equipped with a UHF-RFID tag (COIN ID; 433.92 MHz; 11 g; 36 mm in diameter; 10 mm in thickness; $n = 100$) composed of a mixture of polyurethane resin and corundum (Cassel et al., 2016) were deployed in five patches along a 110-m wide cross-section at the downstream end of HUM1 (Fig. A.1). The artificial cobbles were divided into five patches of 20 tracers with homogeneous grain-size distributions. One patch was deposited directly in the main channel on the right bank, and four patches were deployed on the left-bank gravel bar. They correctly represent the form and density of natural cobbles-pebbles of the site (Table A.2). Five RFID scour chains were also deployed along the cross-section (10 tracers by chain) up to a depth of 1-m below the surface,

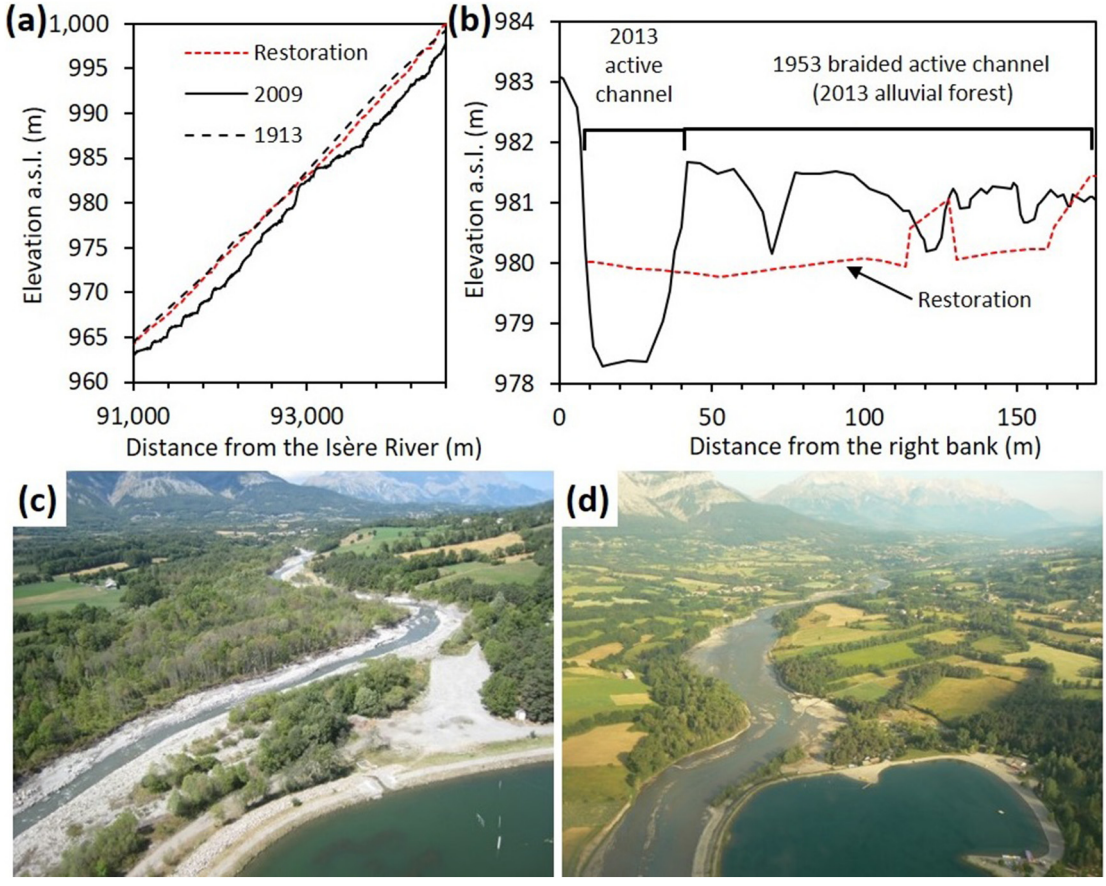

Fig. 2. Historical channel changes and present-day physical restoration of the Upper Drac River; (a) Long profile evolution in HUM3 between 1913 and 2009; (b) A typical cross-section along HUM3 before restoration showing the bed incision into the alluvial fill corresponding to the 1950s braided channel (according to the 1953 aerial photograph); (c) Downstream view of the HUM3 degraded reach in 2011 (ETRM); (d) Downstream view of the same reach in 2014, after restoration (CLEDA); the covered active channels in pictures (c) and (d) correspond to the extent of the restoration project.

following the method described in Brousse et al. (2018). These five RFID columns were used to evaluate the bedload active layer during flow events (Liébault and Laronne, 2008). They have been combined with topographic resurveys of the cross-section with a dGPS (±0.05 m) to constrain the fill depth for each column, and the active width of the cross-section. Accuracies of scour (0.10 m) and fill (0.05 m) measurements give a propagated uncertainty of 0.11 m for the measurement of the active layer depth. Active tags allowed us to detect artificial cobbles and pebbles in surface (range of 80 m according to ELA Innovation©), in subsurface, and below water (e.g., Cassel et al., 2017). Tracer inventories were done according to the quick method (Cassel et al., 2020).

Bedload tracers and RFID scour chains have been used to evaluate the time-integrated bedload flux (V_b in m^3) (Eq. (1)) according to virtual velocity approach (Haschenburger and Church, 1998; Liébault and Laronne, 2008; Mao et al., 2017):

$$V_b = d_b\, W_b\, L_b\, (1-p) \tag{1}$$

with d_b, the active depth of the bed in m (arithmetic mean of scour and fill depths from RFID scour chains included in the active portion of the channel, weighted by the length of active portions in which they are included), w_b, the active width of the bed in m (active portion of the cross-section derived from the combination of information from topographic differencing and RFID scour chains, following the procedure described in Liébault and Laronne, 2008), L_b, the mean travel distance of the artificial cobbles and pebbles in m (considering only mobile tracers), and p, the bed porosity obtained from field measurements according to the protocol described in Bunte and Abt (2001).

This field estimate has been completed with a hydraulic computation of sediment transport by applying a bedload formula to the water discharge record from the Chabottes gauging station (253 km^2), completed for missing values using a linear interpolation with data from the Ricous (207 km^2) and Guinguette (510 km^2) gauging stations. A long profile has been surveyed along a 186-m reach to determine the mean channel slope of the riverbed near the bedload monitoring cross-section (S = 0.0097 m m^{-1}). The surficial grain-size distribution (GSD) was obtained by a classic pebble count (Wolman, 1954) sampling of 100 particles on a lateral bar on the left bank of the cross-section (D_{50} = 0.065 m; D_{84} = 0.099 m). Critical dimensionless shear stress for the bed D_{84} (Recking, 2009) (Eq. (2)):

$$\tau^*_{c84} = 0.56S + 0.021 \tag{2}$$

with S the channel slope in m m^{-1} and dimensionless shear stress (Eq. (3)):

$$\tau^*_{84} = \frac{RS}{(1.65)D_{84}} \tag{3}$$

with R the hydraulic radius (in m), were used to calculate the τ^*_{84}/τ^*_{c84} ratio, which allows to characterize the bedload transport regime (full transport, partial transport, or no motion). The Recking (2013a) formula was used for bedload computation because this formula offers a large field application domain (channel slope from 0.00002 to 0.08 m m^{-1}, and D_{84} from 0.9 to 558 mm) and has been successfully tested with a large bedload dataset collected in the field (Recking, 2013b) (Eq. (4)):

$$Q_b = \rho_s \sqrt{g(s-1)D_{84}^3}\, 14{\tau^*_{84}}^{2.5} \Big/ \left[1 + \left(\frac{\tau^*_m}{\tau^*_{84}}\right)^4\right] \tag{4}$$

with Q_b, the unit bedload transport rate (in g s^{-1} m^{-1}), ρ_s the sediment density, g the acceleration of gravity, s the relative density (ρ_s/ρ with ρ the water density), and τ^*_m the transition between full mobility and partial transport for gravel-bed rivers (Eq. (5)):

$$\tau^*_m = (5S + 0.06)\left(\frac{D_{84}}{D_{50}}\right)^{4.4\sqrt{S}-1.5} \tag{5}$$

3.2. Repetitive LiDAR and terrestrial topographic surveys

Three LiDAR surveys have been used for detecting morphological changes along the study reach. LiDAR1 (September 2015) and LiDAR3 (October 2018) cover the whole study reach, but LiDAR2 (September 2016) covers only HUM3. Technical specifications of the three LiDAR surveys are very similar (Table A.3) and hydrological conditions during the three surveys can be also considered as equivalent (low-flow conditions). The global precision of LiDAR data was measured on immobile targets by the private company in charge of data acquisition. The root mean-square error (*RMSE*) of z values are 0.041, 0.035, and 0.017 m for the three surveys, respectively. Topographic data include only emerged surfaces. In addition, sufficient numbers of echoes are recorded for water surfaces and allow us to interpolate them in each baseflow channel.

Optimization procedure of DoD accuracy (DEM of Difference; 4 pixels m^{-2}) derived from LiDAR data was done by comparison of systematic error (σ_{sys} = mean error) before and after point cloud realignment (Lallias-Tacon et al., 2014; Brousse et al., 2020) on a random set of control points (50%) inside stable surfaces (2 control points m^{-2}). The realignment procedure was done by fixing LiDAR3 as reference because it has the best initial precision. Finally, realignments procedure reduces σ_{sys} for DoD2 and DoD3 but not for DoD1 for which σ_{sys} was initially very low (Table A.4). Volume uncertainty (σ_v) was estimated using the error model of Anderson (2019) (Eq. (6)) that accounted for σ_{sys} and the spatially correlated random errors σ_{sc}:

$$\sigma_v = nL2\sqrt{\frac{{\sigma_{sc}}^2}{n}\frac{\pi\alpha}{5L^2} + \sigma_{sys}} \tag{6}$$

where n is the number of cells, L is the cell size, and α is the range over, which errors are spatially correlated. The magnitude of σ_{sc} was obtained by a semivariogram analysis using 50% of control points. A 50-m regular disaggregation of the study reach using the fluvial corridor toolbox (Roux et al., 2015) allow to extract subreaches in order to reconstruct the longitudinal sediment balance evolution for each DoD.

In addition, since 2013, forty cross-sections are surveyed annually (except in 2017) by classical terrestrial topographic methods using dGPS or a level and a rod. These topographic surveys were used to calculate the spatio-temporal evolution of the morphological signature of the study reach, using the Braided Relief Index (*BRI*; Liébault et al., 2013) (Eq. (7)):

$$BRI = \frac{1}{x_n - x_1}\sum_{i=1}^{n-1}\sqrt{\frac{z_i^2 + z_{i+1}^2}{2}}\,(x_{i+1} - x_i) \tag{7}$$

where z_i is the difference between elevation at x_i and the mean elevation of the cross-section.

The dimensionless BRI (*BRI**) is obtained by (Eq. (8)):

$$BRI^* = \frac{BRI}{W} \tag{8}$$

with W, the active-channel width in m.

These cross-sections were also used to reconstruct the evolution of the low-flow-channel width (W_{lf}) and maximum depth (d_{max}).

3.3. Planimetric evolution using historical aerial photographs and maps

Spatiotemporal evolution of the active-channel width has been reconstructed since the 18th century. Data are derived from historical maps in 1754 and 1857 (Leclair, 2016; with a longitudinal spatial resolution of 25 m) and from historical sets of aerial photos (1953, 1970, 1993, 2003 and 2015; with a longitudinal spatial resolution of 50 m). We used the normalized active-channel width (W^*) of Piégay et al. (2009) in order to compare the morphological

signature of the Upper Drac River with a regional dataset of braided rivers in South-Eastern France. This index is given by (Eq. (9)):

$$W^* = \overline{W_b}/A^{0.44} \quad (9)$$

where $\overline{W_b}$ is the mean active-channel width of the study reach (in m) and A is the drainage area (in km^2).

The surface evolution of macro-habitats after restoration were derived from three sets of orthophotos (2015, 2016 and 2018) by the manual mapping of water surfaces (S_w), alluvial surfaces (S_a), and vegetated surfaces (S_v) of the fluvial corridor. This expert-based photointerpretation was made by the same operator for consistency between dates.

4. Results

Our results describe (i) the evolution of braiding activity since the 18th century, (ii) the bedload supply of the restored reach, (iii) the topographic differencing using airborne LiDAR surveys, and (iv) the morphological trajectory following restoration.

4.1. Evolution of braiding activity since the 18th century

The temporal evolution of the Upper Drac active-channel width (W_b) shows a global narrowing trend since the 18th century. Channel narrowing is relatively less important in HUM1 than in HUM2 and HUM3 (Fig. 3a). Despite channel narrowing, HUM1 conserves a strong braided activity over time ($W^* > 7.5$). This is not the case for HUM2 and HUM3 where narrowing leads to a strong braided activity decrease ($W^* < 3$). In all study reaches, a long-term decrease of W^* is observed with a minimum value in the 1990s and a rebound since the beginning of 2000s (Fig. 3b). This rebound is low in HUM1 (W^* increases from 8.0 to 9.9) and also in HUM2 (W^* increases from 2.4 to 3.4) but strong in HUM3 (W^* increases from 2.6 to 8.8), but this is an artefact related to artificial channel widening of the restored reach.

The recent evolution of the active-channel width (since the early 1970s) can be linked with fluctuations of flood frequency and magnitude (Fig. A.3). The period of active-channel narrowing between 1970 and 1993 is associated with a period of low hydrological activity (19 days > Q_2; 2 days > Q_5), whereas the active-channel widening since the 1990s is concomitant with a period of high hydrological activity (38 days > Q_2; 15 days > Q_5). The recovery of active-channel width observed during the recent active hydrological period can be considered as low, since present-day active channels are still much narrower than in the 1970s. However, the fact that a partial morphological recovery is observed during an active hydrological period let us think that braiding recovery is a coherent management objective for the Upper Drac River.

4.2. Bedload supply of the restored reach

Since the completion of the restoration works, hydrology was not very active with only two small and short-duration floods in September 2015 (flow duration with $Q > Q_2 = 2$ h; instantaneous $Q_{max} = 68.5$ m^3 s^{-1}) and in November 2016 (flow duration with $Q > Q_2 = 6$ h; instantaneous $Q_{max} = 63.8$ m^3 s^{-1}). These flow events were not sufficient to submerge the whole active channel of the restored reach. As a consequence, morphological adjustments were likely less driven by the rainfall-induced flood regime than by the snowmelt flow regime.

Since January 2017, three bedload tracer and RFID scour chain inventories have been carried out concomitantly in August 2017 (S1), December 2017 (S2), and September 2018 (S3; Table A.5). Concerning bedload travel distances, all of the tracers belonging to the 32–45 mm class ($n = 25$) were never detected. Two reasons can be proposed to explain this detection problem: (i) UHF tags of the finest tracers had to be mechanically reduced in diameter and this could have damaged the RFID components; (ii) the small quantity of resin used to make these small

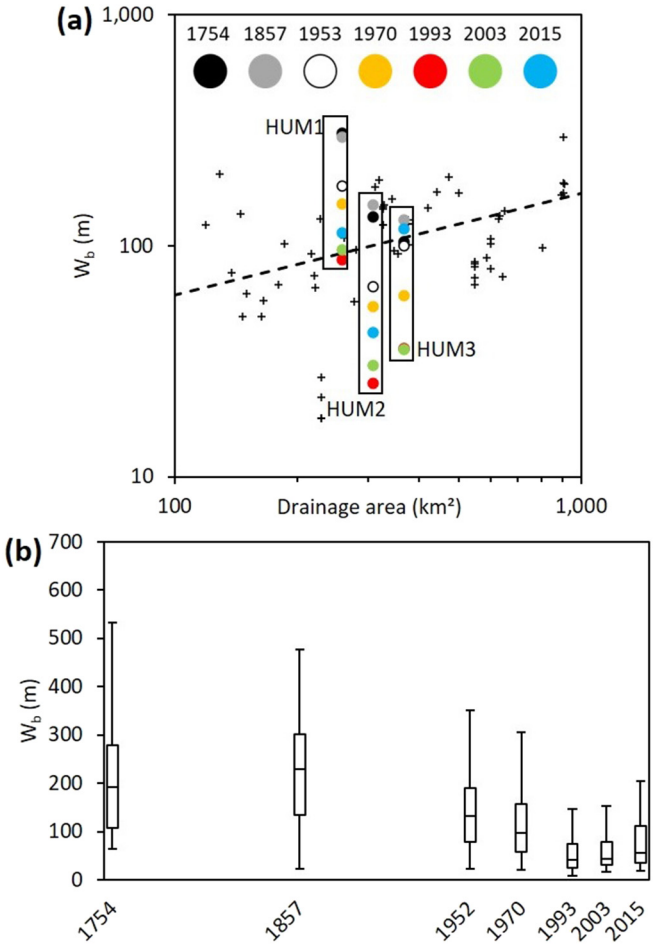

Fig. 3. Spatio-temporal active-channel evolution of the Upper Drac River between 1754 and 2015; (a) Active-channel evolution compared to the regional dataset of braided rivers in SE France, from Piégay et al. (2009); the dotted line represents a linear adjustment ($y = 8.05\ x^{0.44}$) and illustrates the limit for separating active from inactive braided rivers; black cross: data from Piégay et al. (2009); (b) Active-channel evolution at the study reach scale; from the bottom to the top, each box plot segment represent 10th, 25th, 50th, 75th and 90th percentiles (outliers values are not represented to simplify the figure).

artificial cobbles could have induced a higher water infiltration in the tracer, and their subsequent deterioration by frost. The second explanation is likely the best, since the tags have been well-detected in the laboratory once molded in their artificial pebbles. Anyway, this set of small-sized tracers has been removed from the analysis. For other tracer classes, the recovery rates based on the total number of tracers is very high (79 to 97%; Table A.5). However, the recovery rates of mobile tracers are lower and show a strong decrease over time, from 80% to 36% between the first and the last inventories. Bedload travel distances show a rapid dispersion of tracers through HUM2 (Fig. 4a). In December 2017, only eleven months after the deployment of tracers, frontrunners had been transported over more than 1 km and were found in the upstream section of the restored reach. This clearly shows a rapid bedload transfer from the Chabottes braided reach (HUM3) to the restored reach (HUM1). A strong effect of the initial tracer position in the cross-section on mobility is observed. Tracers deployed in the main channel show a much higher mobility rate (93.5%) than tracers deployed on the gravel bar (0.5%). The mean annual bedload transport distance obtained from tracers deployed in the main channel is about 1 km a^{-1}. Travel distance is controlled by the grain-size attesting a selective transport condition.

Bedload active layer monitoring for S1 indicates a lateral migration of the main channel of around 12 m towards the left bank and a partial filling of secondary channels (Fig. 4b). The next survey (S2) does not show any significant morphological activity along the cross-section,

while the last survey (S3) shows the scouring of the main channel and erosion of the bar. On the left side of the cross-section, we detected the creation of a new secondary channel. These topographic surveys clearly indicate a much higher morphological activity in the main channel and its vicinity, and only minor changes in the gravel bar. The average active layer depth of each RFID scour chain ranges from 0.05 m to 0.24 m, with a global mean of 0.13 m (±0.11 m) over the entire period (Table A.6). The active width remained small (58 m for S1, 31 m for S2, and 52 m for S3), which illustrates a partial remobilization of the active channel. Maximum active layer depths are observed at C1 (0.45 m) and at C5 (0.12 m). Other RFID scour chains show a marginal active layer depth (<0.05 m). Single scouring of C1 (0.70 m) during the first survey, illustrates lateral erosion as a control factor of active layer during the 2017 snowmelt. However, scouring of C1 (0.20 m) and C5 (0.10 m) during the third survey illustrates the importance of vertical erosion processes during the 2018 snowmelt.

Results from the bedload active layer monitoring show a higher morphological reworking of the channel for the 2017 snowmelt, whereas the 2018 snowmelt was hydrologically more active. In fact, total runoff was two times higher during the 2018 snowmelt (Fig. A.4). The maximum 2017 snowmelt peak flow ($Q_{max} = 26.6\ m^3\ s^{-1}$) has been exceeded over 18 days during 2018 snowmelt ($Q_{max} = 37\ m^3\ s^{-1}$). Due to hydrological difference between both snowmelt periods, it is possible that the number of channels was higher in 2018 than in 2017, suggesting a higher specific stream power in 2017. As a consequence, the 2017 snowmelt was likely more favorable to lateral erosion.

The virtual velocity approach allows estimating a total bedload supply of 9966 m^3 between January 2017 and September 2018 (Table A.7). According to hydraulic computations, the critical dimensionless shear stress of the D_{84} has been exceeded 22.8% of the time from September 2015 to October 2018 (period of topographic differencing using airborne LiDAR data) and 25% of the time from January 2017 to September 2018 (period of bedload monitoring using tracers and RFID scour chains). For both periods, the total bedload transport volumes obtained from hydraulic computations were 17,000 m^3 and 11,450 m^3, respectively (Fig. A.4).

4.3. Topographic differencing using airborne LiDAR surveys

The DoD between September 2015 and October 2018 shows a negative sediment balance in HUM1 ($-6400 \pm 173\ m^3$) and a positive sediment balance in HUM2 ($5400 \pm 30\ m^3$). When these two reaches are considered as a whole, it appears that the 10-km river length upstream of the restored reach has been subjected to a net sediment loss during the 3-years monitoring period. This is consistent with the net aggradation observed during the same period in HUM3 ($11{,}800 \pm 93\ m^3$). Longitudinal variations of the net sediment balance show much higher deposition and erosion processes in HUM1 and HUM3 than in HUM2 (Fig. A.5a). This suggests that bedload is passing through HUM2 without strongly interacting with the channel morphology, and that this confined reach is likely functioning as a rapid sediment conveyor belt. A classic alternating pattern of erosion and deposition subreaches is observed along HUM1 and HUM3, with a mean spacing of about 215 m ($\sigma = 156$ m). Sequential DoDs show a moderate evolution between 2015 and 2016 and a stronger activity after 2016 (Fig. A.5b; Table 1). This highlights the impact of the November 2016 flood and both snowmelt periods. Sediment loss in the upper restored reach is continuous over the survey period, and aggradation in the middle part of the

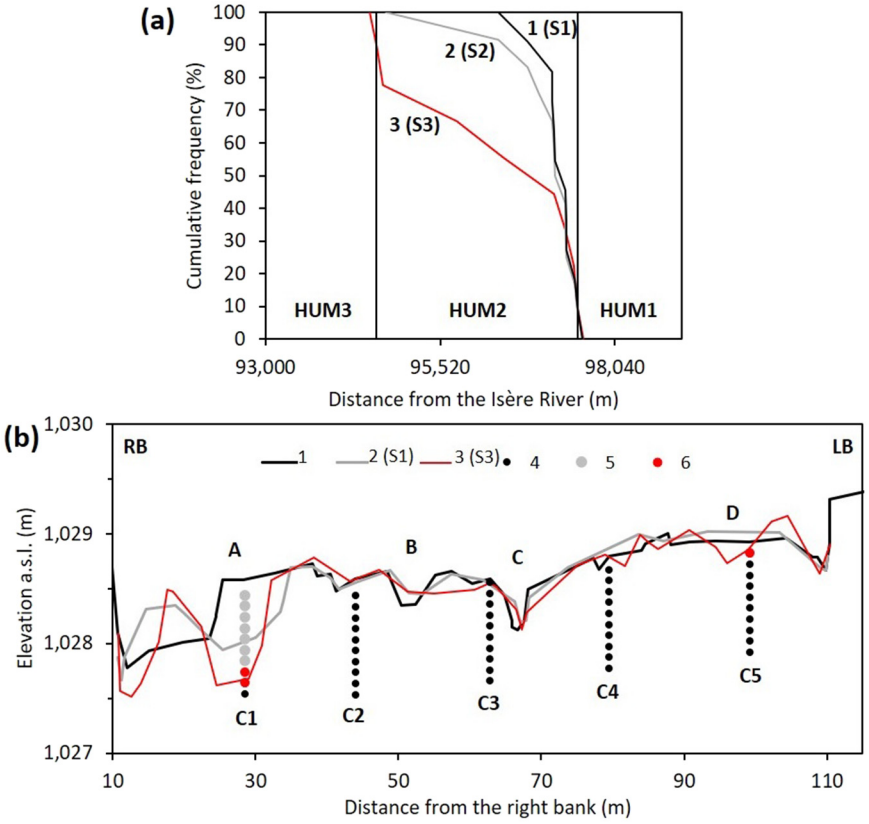

Fig. 4. Bedload transport distance and active layer thickness data in the Upper Drac River between January 2017 and September 2018; (a) Bedload transport distance; Curve represent cumulative frequency distributions of bedload tracer transport distances; 1: August 2017 (S1); 2: December 2017 (S2); 3: September 2018 (S3); (b) Topographic changes of the Upper Drac River at the surveyed cross-section between January 2017 and September 2018, including active layer thickness data from RFID scour chains; 1: topographic survey in January 2017; 2: topographic survey in August 2017 (S1); 3: topographic survey in September 2018 (S3); 4: stable RFID tracers; 5: remobilized RFID tracers in August 2017; 6: remobilized RFID tracers in August 2018; A: main channel lateral mobility and scouring; B and C: secondary channel partial filling; D: sediment deposition on gravel bar and scouring of a secondary channel.

Table 1
Sediment balance of the Upper Drac River between 2015 and 2018; values in brackets represent the percentage of water surface in the active channel.

DoD	Reach	Systematic error (m)	spatially correlated random errors (m)	Net sediment balance of the active channel (m^3)	Net sediment balance of exposed surfaces (m^3)	Net sediment balance of submerged surfaces (m^3)
09/2015–10/2018	HUM1	−0.0003	0.045	−6400 ± 173	20,600 ± 151	−27,000 ± 22 (12.5)
	HUM2	−0.0003	0.045	5400 ± 30	8900 ± 17	−3500 ± 14 (44.3)
	HUM3	−0.0003	0.045	11,800 ± 93	20,800 ± 67	−9000 ± 27 (28.7)
09/2015–09/2016	HUM3	−0.0045	0.035	1200 ± 1486	4100 ± 774	−2900 ± 712 (50.0)
09/2016–10/2018	HUM3	0.0016	0.052	11,500 ± 518	18,800 ± 372	−7300 ± 155 (28.7)

restored reach is not really visible before 2016. The lower morphological activity in the downstream part is observed for both periods.

Topographic differencing along the restored reach reveals a substantial spatial variability of morphological changes (Fig. 5a). The upstream part of the restored reach is characterized by a net incision [from kilometric point (KP) 94.4 to KP 93.3]. This subreach is characterized by the formation of a well-shaped channel and tends to adopt a wandering pattern. This evolution seems to be controlled by upstream erosion propagation, which was initiated in the transition between this confined subreach and the less confined downstream subreach and in a sector of local slope increasing (Fig. 5b). Downstream of this incised sector, an aggraded sector (from KP 93.3 to KP 92) interrupted by two local incision zones (KP 92.8 and KP 92.4) is observed. In this sector, the positive sediment balance is driven by accretion of gravel bars (Fig. 5c). The downstream end of the restored reach is characterized by a small net incision. Sequential DoDs show a moderate evolution between 2015 and 2016 and a stronger activity after 2016. This highlights the impact of the November 2016 flood and the 2017 snowmelt. Sediment loss in the upper restored reach is continuous over the survey period, and aggradation in the middle part of the restored reach is not really visible before 2016. The lower morphological activity in the downstream part is observed for both periods.

4.4. Morphological trajectory following restoration

The evolution of macro-habitats between 2015 and 2018 in the restored reach shows a rapid and continuous growth of vegetation units, from 6% in 2015 to 29% in 2018, to the detriment of water units, which decrease from 39% to 22% with a negligible discharge difference (delta of 0.5 $m^3 s^{-1}$ at the Ricous gauging station; Fig. A.6). Unvegetated sediment units are stable and remain the dominant habitat over the period. The spatial pattern of habitats tends to become more complex through time with the vegetation encroachment along the active-channel margins and banks in the widest subreaches. The spatial heterogeneity of habitats increases, with a greater lateral and longitudinal diversity. A fragmentation of the active channel is observed because of the combined effects of the channel network development and vegetation establishment on bars. This mosaic of habitats is getting closer to the reference conditions (HUM1). However, in 2018, only water surfaces are well adjusted whereas vegetated and unvegetated sediment units are not. This is explained by the size of the wooded islands of HUM1 (3 ha, KP 92.1), which represents 22% of the vegetated areas. This type of large wooded islands is not found in the reference reach.

The comparison of the morphological signatures of the restored reach with the Chabottes reach reveals a clear trajectory towards reference physical conditions. In 2015, the median baseflow channel width in HUM3 (14.5 m) was 2.7 times greater than in HUM1 (5.5 m), while in 2018 this ratio was only 1.4 (Fig. 6a). A decrease in the standard deviation of this metrics is also observed over time. In the meantime, the median of the low-flow channel depth increases from 0.18 m to 0.60 m (Fig. 6b) but this index is still lower than the reference value (0.80 m). The continuous increase in standard deviation of this metrics suggests that adjustments of the channel geometry are not achieved.

The BRI^* index indicates a constant increase since the restoration (Fig. 6c), with values close to the reference reach in some cross-sections (0.0045; Lallias-Tacon, 2015). However, the majority of the cross-sections of HUM3 are characterized by a BRI^* lower than the reference condition. The spatiotemporal evolution of the BRI^* index shows that the adjustment to the reference value is faster upstream of HUM3 than downstream (Fig. 6d). Moreover, whatever the period considered, the linear regression of the BRI^* index as a function of the longitudinal distance is characterized by a negative slope. Correlation remains low or marginal, which suggests that the longitudinal distance is not the only factor controlling the longitudinal evolution of the BRI^*.

5. Discussion

5.1. How reliable are sediment balances derived from sequential LiDAR data?

Data processing of sequential LiDAR surveys of the Upper Drac River shows that point cloud realignment strongly improves the reliability of mass balance computation by reducing the systematic error on stable patches, as already demonstrated by several case studies in gravel-bed rivers (Lallias-Tacon et al., 2014; Anderson, 2019). This pre-processing step is crucial when topographic differencing is covering a wide spatial extent of braided channels. Similar hydrological conditions between our LiDAR surveys also improve the comparability of elevation models over time. However, ignorance of bathymetry prevents to give full confidence in the sediment balances due to potential underestimation of erosion and deposition under water surfaces. In addition, this potential bias strongly depends on the relative area of water surfaces in the active channel, which is not homogeneous along the study site. Detailed sediment balance for submerged surfaces (Table 1) and their relative area in active channel show evident longitudinal heterogeneity. In HUM1, the sediment balance can be considered as weakly impacted by the water surfaces, which represent only 12.5% of the active channel, but not in HUM2 were water surface represent 44.3% of the active channel, which could easily reverse the positive sediment balance. In HUM3, underestimation of erosion in baseflow channels is possible, but this is likely not reversing the positive sediment balance. Indeed, most of the deposits took place in the middle wide sector of HUM3, in which the evolution of the low water surface is much less important than everywhere else in the restored reach. Consequently, if incision processes could have taken place under the water surfaces, these must have been limited. Moreover, decreasing water surfaces since 2014 allow reducing sediment balance uncertainty over time. We can therefore give a good confidence to the sediment balance of HUM3.

5.2. How efficient are the restoration works to stop channel incision and recreate a braided channel?

Massive gravel replenishment and channel widening allowed stopping the rapid channel incision of the Upper Drac River, as shown by the net positive sediment balance of the restored reach after restoration. In this particular context of low hydrological forcing after restoration, sediment delivery to the restored reach as well as the general morphological activity of the river should be considered of moderate intensity. However, remarkable scouring processes are observed locally along the restored reach 3–4 years after the replenishment, notably along the two most confined and steepest sub-reaches. This is not surprising, since those segments exhibit maximum shear stress levels during flow events. Those particularly active scouring zones have then provided

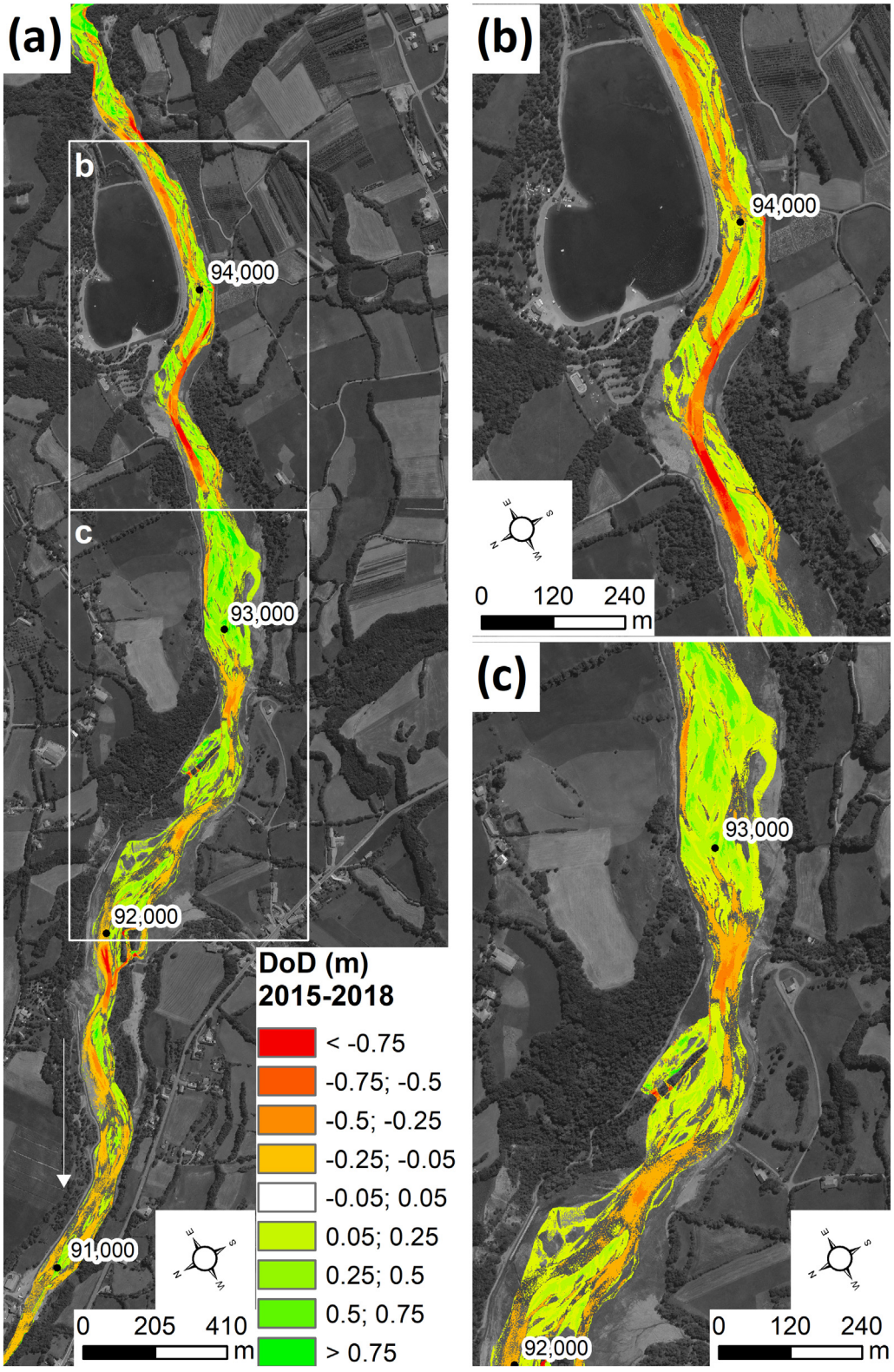

Fig. 5. Channel change detection map from sequential airborne LiDAR surveys over the survey period (2015–2018) in the Upper Drac River; (a) Global map of HUM3; (b) Zoom in the incised subreach; (c) Zoom in the aggraded reach.

sediment downstream and have contributed to the braiding development along the wider portions of the active channel. This may have counterbalanced the low sediment supply from upstream, related to the hydrological context. Nevertheless, if channel incision persists in these critical spots, there will be a great risk of clay deposit breakthrough, meaning of total failure of this emblematic restoration project. Is such a risk a likely outcome? It is quite difficult to answer, because it is still unclear if the scouring of the confined reaches should be seen as a local adjustment of the long profile into a succession of sedimentation and transfer zones (sensu Church and Jones, 1982), which is a common longitudinal pattern of braided rivers, or if the scouring corresponds to the initiation of a shift towards the single-thread pattern prevailing

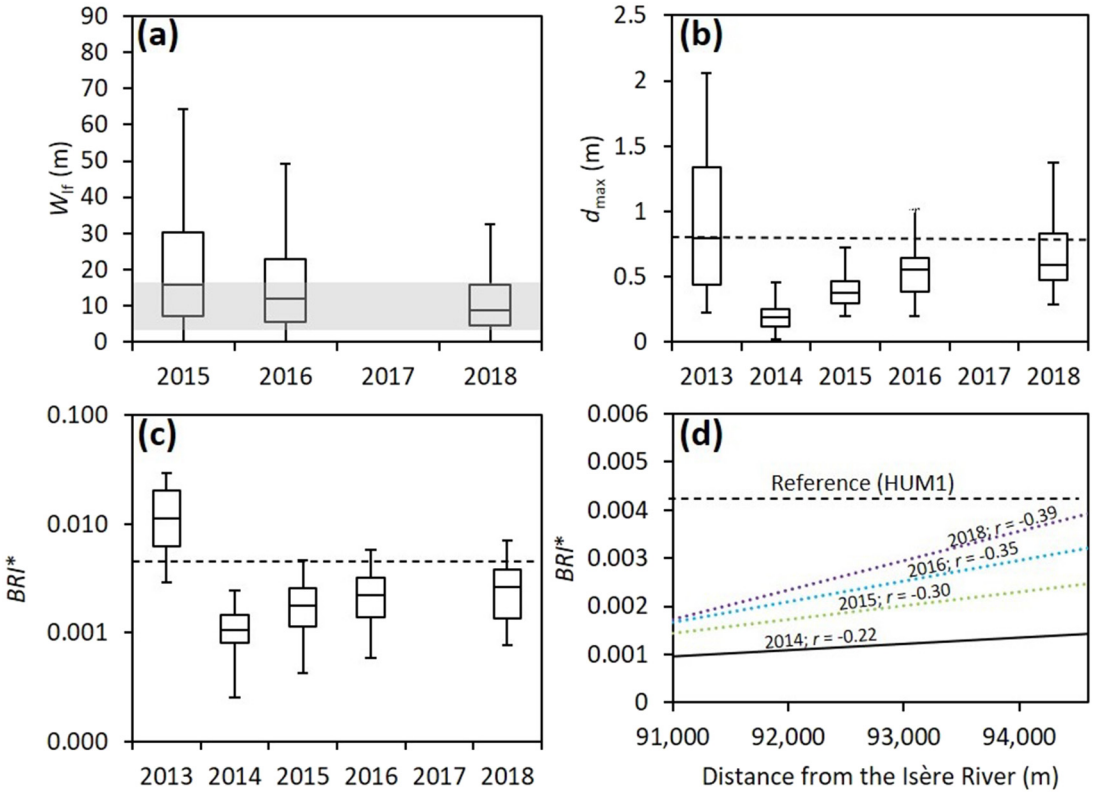

Fig. 6. Morphometric adjustments of the restored reach of the Upper Drac River; (a) Low-flow channel width evolution; grey surface represents the standard deviation of the low-flow channel width in the reference reach (HUM1); (b) Evolution of the maximum depth of low-flow channels; the dotted line represents the reference value in HUM1 according to Misset (2019); (c) Dimensionless Bed Relief Index (*BRI**) evolution; the dotted line represents the reference value in HUM1 according to Lallias-Tacon (2015); (d) Longitudinal evolution of the *BRI** according to linear regression curves. Each box plot segment represents 10th, 25th, 50th, 75th and 90th percentiles (outlier values are not represented to simplify the figure).

before restoration (confined wandering pattern). It is therefore of uppermost importance to maintain the morphological monitoring of the restored reach in the near future, for adaptive management purposes (Downs and Kondolf, 2002). In the event of spreading of the scouring zones along the unconfined braided portions of the restored reach in the near future, it should be recommended to implement a new operation of gravel replenishment. This can be justified by the lag time between the cessation of gravel mining in the Chabottes plain, and its effect on the sediment supply of the restored reach. However, it will certainly not be a viable management strategy to reproduce such operations on a regular basis, as this would be considered as a wasted effort against the "natural" evolution of the river.

Whatever the future trajectory of these two entrenched reaches, this case study shows that the risk of clay breakthrough still exists and that

Fig. 7. Downstream view of the Upper Drac River restored reach in 2018, showing the spontaneous recovery of the braided channel morphology (©SIGosphère).

anticipating potential vertical erosion of around 1–2 m in the first years after restoration is a key point to consider when designing the recreation of an alluvial cover above a substrate sensitive to scouring. Another point relies upon the fact that channel aggradation is observed along every unconfined portions of the bed. This observation highlights the need to combine replenishment and channel widening for improving morphological conditions. Local slope increases have also a great importance in the channel incision process, since these are potential starting points of regressive or progressive erosion, as observed along the restored reach. These zones should be monitored in priority after restoration if it is not possible to survey the whole restored reach during the post-restoration monitoring program.

Spontaneous braided pattern recovery has been particularly efficient along the restored reach as shown by the rapid and continuous development of a multi-thread channel pattern with active gravel bars right few years after the restoration works (Fig. 7). From a purely aesthetical point of view, the restoration project can be considered as a real success. The effective braiding recovery is also documented by low flow channel width decreasing, low-flow channel depth and *BRI** index increasing, which highlights the strong morphological adjustment capacity of the Upper Drac River despite the relatively low hydrological activity. Our results attest to the possibility to skip the step of channel shaping during works and to the spontaneous development of a multi-thread network after bed widening and rising. However, even if morphological adjustments are fast, the braided pattern do not adjust exactly to the reference conditions in the Chabottes plain, which suggest that the recovery of the restored reach is not finished.

5.3. Is braided pattern recovery sustainable?

The sustainability of the restored braided pattern of the Upper Drac River is supported by several observations. At the valley scale, a rapid bedload transfer between the Chabottes plain and the restored reach (1 km a^{-1}) is observed, showing efficient sediment connectivity with the main proximal sediment source of the restored reach. At the reach scale, we can expect that the cessation of gravel mining since 2012 has improved the sediment transport continuity along the river. In fact, the ancient gravel mining site downstream HUM1 was able to temporarily trap an important part of the bedload increasing downstream sediment deficit. However, this mining pit is definitively filled, which should result in the restoration of natural sediment waves propagating from the Chabottes plain to the restored reach. When distal sediment sources are considered, it appears that several active torrents are feeding the Drac River with coarse material. At least five torrents with strong evidences of important coarse sediment delivery to the mainstem (by debris flows or bedload transport) are identified at a distance (river length) of less than 20 km from the restored reach. Sediment supply from the floodplain is also well preserved along the mainstem, where bank protections are restricted to less than 20% of the cumulative bank length. It has been shown that present-day conditions of sediment supply from active torrents and bank erosion are of critical importance for explaining morphological trajectories of Alpine braided rivers (Liébault et al., 2013). The comparison of the Upper Drac with other Alpine braided rivers in SE France clearly reveals that its sediment supply conditions can be considered as favorable for the preservation of a braided pattern.

The historical perspective of the Upper Drac morphological trajectory brings also some insights into the question of braided pattern sustainability. Historical active channel narrowing is a common pattern for Alpine braided rivers (Liébault and Piégay, 2002; Surian and Cisotto, 2007; Comiti et al., 2011; Lallias-Tacon et al., 2017), and the Upper Drac River follows the general trend resulting from the cumulative impact of sediment supply decrease from catchments and human disturbances on sediment transport. However, it is interesting to see that the braided reach of the Chabottes plain still presents today a high normalized active channel width, which is above the regional threshold value separating wide and narrow braided rivers (Piégay et al., 2009). This is even more noteworthy when we consider the persistence of intensive gravel mining until 2012 along this river. The fact that active channel widening is observed along the Upper Drac River during the last active hydrological period that started in the early 1990s is also confirming the strong recovery potential of the braided channel. This historical perspective finally confirms what has been previously inferred from the analysis of present-day conditions of sediment supply and connectivity from the Upper Drac catchment.

However, the fact that the Upper Drac catchment is able to maintain active braided channels along some reaches does not necessarily mean that braiding is a sustainable fluvial pattern along the restored reach itself. The simple fact that the braided pattern disappeared along this reach in the 1970s, and not in the Chabottes plain, reveals that local conditions can strongly control morphological trajectories. It is hard to believe that the contrasting evolution between HUM1 and HUM3 is related to different levels of human pressures, since gravel mining has been operating on both sites. The main difference which can be seen as relevant for explaining their contrasted morphological responses is the sedimentology of the valley floor. A much higher thickness of the post-glacial alluvial fill is observed in the Chabottes plain (around 50 m) than in the restored reach (around 5 m; B.I.G., 1979). Therefore, channel incision in the restored reach rapidly cut through ancient fluvio-lacustrine clay deposits, and this outcropping has a positive feedback on channel incision by increasing the scouring rate and by reducing gravel supply from bank erosion. This sedimentological specificity of the restored reach likely explains its high sensitivity to disturbance, and the challenging nature of braided restoration along this singular reach. However, the fact a braided channel existed there in the 1950s, as attested by the oldest aerial photos, proves that this objective of restoration makes sense now that gravel mining has stopped.

6. Conclusion

The monitoring of the physical restoration of the Upper Drac River clearly reveals a very efficient spontaneous recovery of braiding conditions along the 3-km widened and replenished river reach, in a general context of low hydrological forcing. Post-restoration monitoring shows that the initial uniformly flat alluvial platform rapidly evolves towards a typical braided channel with a mosaic of active gravel bars separated by multiple anabranches. From a purely aesthetic point of view, this restoration is a real success, as today, the restored reach really looks like a "natural" braided river reach. Bedload tracing experiment confirm a rapid dispersion of gravels from the main upstream sediment reservoir of the restored reach. This strong coarse sediment connectivity is a positive point for the resilience of the braided pattern in the restored reach. It is however difficult to make any definitive conclusion about the future morphological trajectory of the reach, and notably the risk for local channel scouring observed along the confined portions of the active channel to persist over time and to propagate along the reach. It is therefore of uppermost importance to maintain the morphological monitoring in the near future, for adaptive management purposes.

This study confirms that the combination of massive gravel replenishment and channel widening can be an efficient management strategy to restore braiding in mountainous catchments. Despite the need to apply this strategy to catchment with high sediment production and good sediment continuity to ensure sustainability, efficiency of braiding restoration depends on the definition of three main parameters: slope, active-channel width and replenishment thickness. Some recommendations could be proposed to managers who plan to use similar strategy of restoration: (i) first, a great care should be taken to morphological trajectory before planning braiding restoration in order to anticipate project feasibility, efficiency and viability; (ii) second, it is necessary to design a channel with regular slope and width along the reach to avoid local scouring and subsequent regressive or progressive erosion; (iii) third, in case of design with irregular slope or width, scouring has to be anticipated (around 1–2 m in our case) by enforcing

replenishment thickness at each slope inflection point and confined sub reaches; (iv) fourth, managers have to follow adaptive management and monitoring after restoration in order to adapt to morphological adjustments.

CRediT authorship contribution statement

Guillaume Brousse: Conceptualization, Methodology, Investigation, Visualization, Formal analysis, Writing - original draft. **Frédéric Liébault:** Validation, Supervision, Conceptualization, Writing - original draft. **Gilles Arnaud-Fassetta:** Project administration, Writing - review & editing. **Bertrand Breilh:** Resources. **Sandrine Tacon:** Data curation.

Declaration of competing interest

The authors declare that they have no known competing financial interests or personal relationships that could have appeared to influence the work reported in this paper.

Acknowledgements

This work benefited from the financial support of the INTERREG Alpine Space HyMoCARES project, Office Français de la Biodiversité (OFB) and from the logistical support of the Communauté Locale de l'Eau du Drac Amont (CLEDA). We thank Mathieu Cassel (EVS, UMR 5600) for technical help during artificial cobble-pebble manufacturing and Xavier Ravanat (INRAE) for his help in the field during deployment of RFID scour chains. Colleagues from the Conseil Départemental des Hautes-Alpes (Romain Gaucher and Isabelle Chouquet) and from hydraulic engineering private companies (Frédéric Laval from BURGEAP and Vincent Koulinski from ETRM) are acknowledged for the general discussions and advices about the restoration project and the field monitoring program. Alain Recking (INRAE) and Mélanie Bertrand (INRAE) are acknowledged for advices in bedload-transport computation and GIS data processing, respectively. We wish to thank the Editor and the four anonymous referees for their careful reviews which helped us to improve the manuscript.

Appendix A

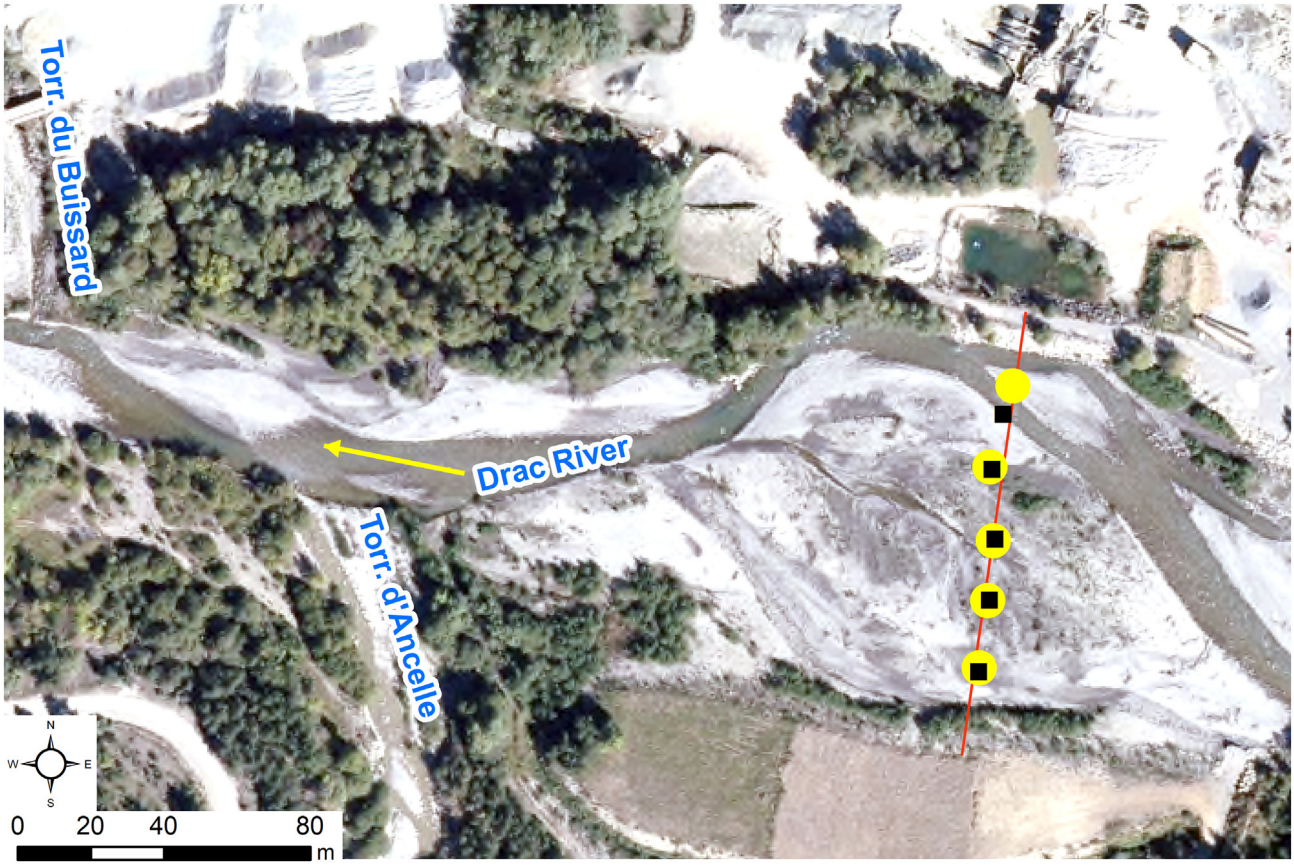

Fig. A.1. Location of artificial cobble-pebble tracers and scour chain at the downstream end of HUM1, Upper Drac River; yellow circles, dark squares and the red line represent tracer patches, RFID scour chains and the monitored cross section, respectively; background: October 2018 aerial orthophoto.

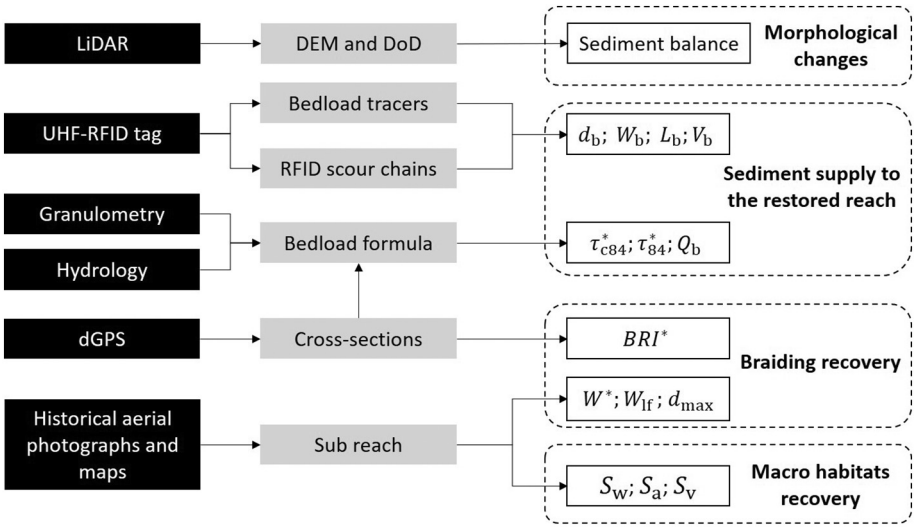

Fig. A.2. Flowchart of the physical monitoring used to investigate the morphological trajectory; dark, grey, white and dashed box represent material, derived application, derived index and monitoring objectives, respectively.

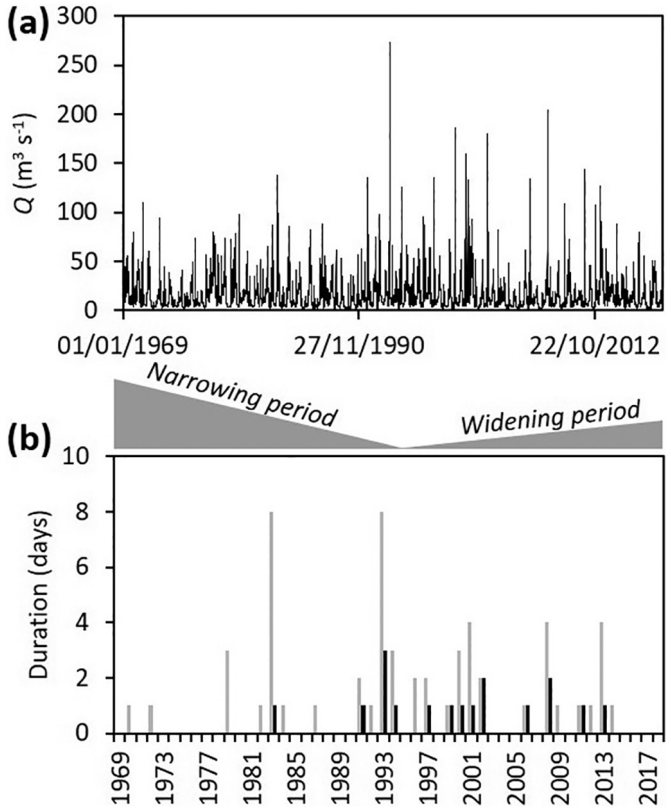

Fig. A.3. Hydrological record of the Upper Drac River at the Guinguette gauging station, which is the longest available hydrological time series of the catchment; (a) time series of the mean daily discharge since 1969; (b) duration of Q_2 (grey bars) and Q_5 (dark bars) daily flood discharges by year between 1969 and 2018.

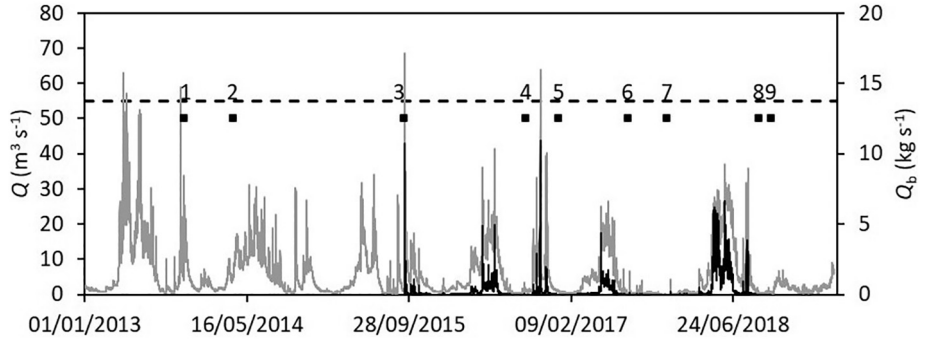

Fig. A.4. Instantaneous water discharge record and associated bedload transport computation of the Upper Drac River upstream of the restored reach; the grey line represents water discharges at the Ricous gauging station and the dotted line represents the Q_2 instantaneous discharge; the black line corresponds to bedload computation at the Chabottes gauging station, starting in September 2015; 1: beginning of the restoration; 2: end of the restoration; 3: LiDAR1; 4: LiDAR2; 5: tracer deployment; 6: RFID survey 1; 7: RFID survey 2; 8: RFID survey 3; 9: LiDAR 3.

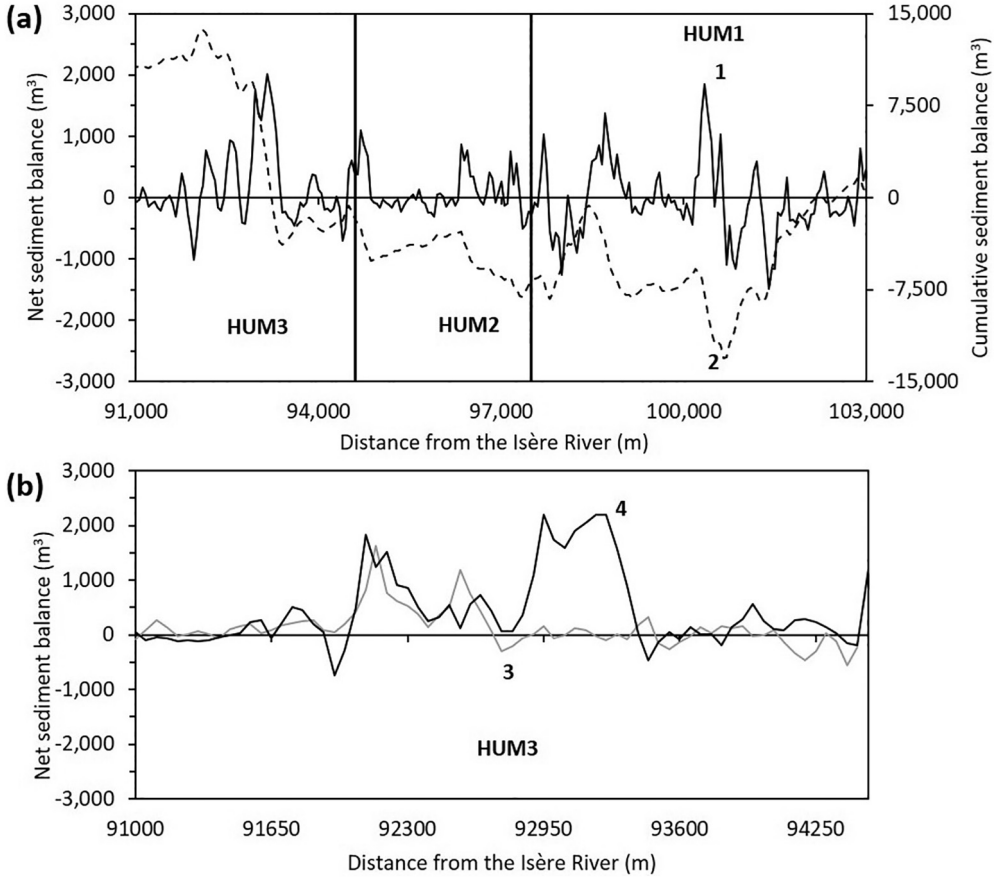

Fig. A.5. The sediment balance of the Upper Drac River derived from topographic differencing using sequential airborne LiDAR surveys; (a) global longitudinal sediment balance between 2015 and 2018; 1: net sediment balance by disaggregated 50-m subreaches; 2: cumulative net sediment balance. (b) Net sediment balance of the restored reach; 3: net sediment balance between 2015 and 2016; 4: net sediment balance between 2016 and 2018.

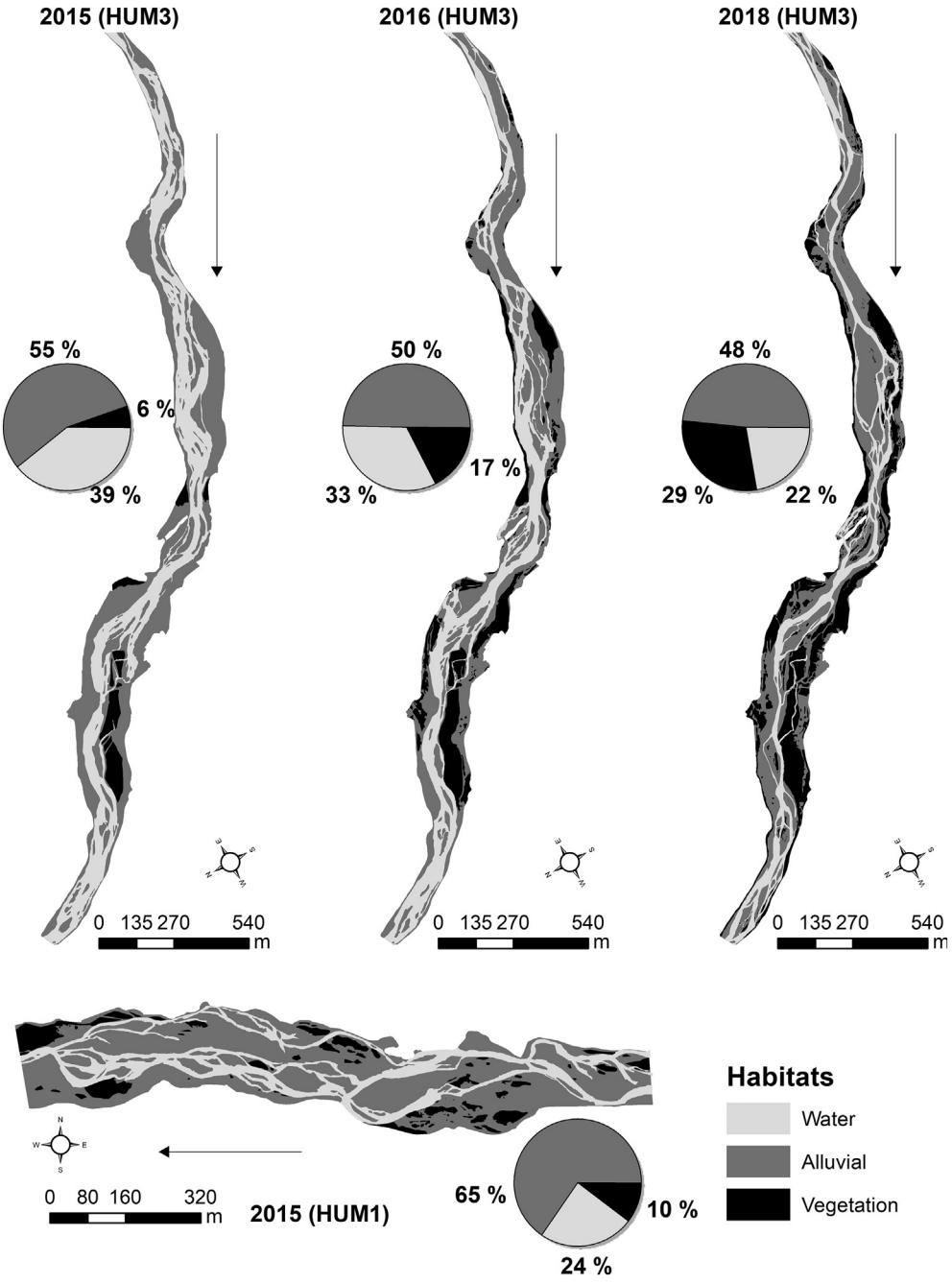

Fig. A.6. Macro habitat evolution of the Upper Drac River restored reach (HUM3) between 2015 and 2018; the reference site (HUM1) correspond to a very well-preserved braided reach (Chabottes plain) upstream of the restored reach.

Table A.1
Main characteristics of the three study reaches of the Upper Drac River.

Study reach	Length (km)	Mean active-channel width (m)	Area (ha)[a]	Channel slope (%)
HUM1	7	96	96	1.19
HUM2	2.9	30	16.2	0.91
HUM3	4.2	35	50.4	1.04

[a] Area of the active channel.

Table A.2
Characteristics of artificial cobbles-pebbles equipped with active UHF-RFID tags in the Upper Drac River.

Grain-size class (mm)	[32–45]	[45–64][a]		[64–90][a]		[90–128]
A-axis (mm)	45.5	74	63	84	90.5	135
B-axis (mm)	44.5	47	59.5	68	72.5	109
C-axis (mm)	29	35.5	28	41	39.5	58
Mass (g)	77.6	178.8	151.3	356.4	383	1134.4
Volume (cm^3)	29.1	68.5	57.2	132.6	145.4	428.3
Density	2.67	2.61	2.65	2.69	2.63	2.65
Number of particles	25	12	13	12	13	25

[a] For these grain-size classes there are two different shapes of artificial cobble pebbles.

Table A.3
Technical specifications of airborne LiDAR data acquisitions in the Upper Drac River.

Date	LiDAR1 9/10/2015	LiDAR2 10/22/2016	LiDAR3 10/18/2018
Laser	Riegl LMS Q680i	Riegl LMS Q680i	Riegl LMS-Q780
Flight height (m above ground level)	580	550	650
Flight speed (nd)	80	70	97
Scan frequency (kHz)	400	400	400
Altimetric accuracy (m)	0.1	0.08	0.1
Planimetric accuracy (m)	0.25	0.25	0.075
Point density (point m^{-2})[a]	5.2	11.0	12.0
Ground control points	180	376	180
RMSE (m)	0.041	0.035	0.017
Discharge at the Ricous gauging station (m^3 s^{-1})	0.96	1.17	0.43

RMSE: root mean square error.
[a] Point density after filtering vegetation and water echoes.

Table A.4
3D point cloud realignment and effect on systematic error.

DoD	Systematic error (m)		Control points
	Initial point cloud	Realigned point cloud	
DoD1 (LiDAR1-LiDAR2)	−0.004	−0.00637	67,489
DoD2 (LiDAR2-LiDAR3)	0.013	0.00163	119,301
DoD3 (LiDAR1-LiDAR3)	0.013	−0.00029	77,471

Table A.5
Summary reports of results from the bedload tracing program using UHF RFID active tags in the Upper Drac River.

Survey	Recovery rate (%)[a]	Mobile tracers (%)	Mean distance of transport (m)	Maximum distance of transport (m)	Cumulative mean distance of transport (m)	Cumulative maximum distance of transport (m)
August 2017 (S1)	72/75 = 0.96 (12/15 = 0.80)	12/72 = 0.17	440	1276	440	1276
December 2017 (S2)	73/75 = 0.97 (3/5 = 0.60)	3/73 = 0.04	1037	2894	646	2894
September 2018 (S3)	59/75 = 0.79 (9/25 = 0.36)	9/59 = 0.15	852	2702	1328	3121

[a] In brackets, recovery rates for mobile tracers only.

Table A.6
Summary report of results from active layer survey using RFID scour chains and cross-section resurveys in the Upper Drac River; d_b: active layer depth; Δ_h: net topographic change from cross-section resurvey; W_b: active width; *scour values obtained from cross-section resurveys (no scour detection from RFID scour chains, due to insufficient measurement resolution); in bold: RFID scour chains included in the active width of the channel, and used for the computation of the mean active depth for each period.

Survey		C1	C2	C3	C4	C5	Active width (m)	Mean active layer for active width (m)
August 2017	Scour (m)	**0.7**	0	0	**0**	**0**	58	0.24
	Fill (m)	**0.21**	0.02	0.01	**0.1**	**0.1**		
	Active layer (m)	**0.45**	0.01	0	**0.05**	**0.05**		
	Topographic difference (m)	**−0.49**	0.02	0.01	**0.1**	**0.1**		
December 2017	Scour (m)	0	0	0.05*	**0.09***	**0**	31	0.05
	Fill (m)	0.04	0	0	**0**	**0.13**		
	Active layer (m)	0.02	0	0.02	**0.04**	**0.06**		
	Topographic difference (m)	0.04	0	−0.05	**−0.09**	**0.13**		
September 2018	Scour (m)	**0.2**	0	0	**0.07***	**0.1**	52	0.1
	Fill (m)	**0.04**	0.03	0.01	**0**	**0.15**		
	Active layer (m)	**0.12**	0.01	0	**0.03**	**0.12**		
	Topographic difference (m)	**−0.16**	0.03	0.01	**−0.07**	**0.05**		

Table A.7
Estimation of coarse sediment supply at the downstream end of HUM1 from the active layer and transport distance in the Upper Drac River; a constant bed-material porosity of 0.23 has been considered for bedload volume computation; the value in brackets represent the mean annual bedload supply rate.

Period	Active width (m)	Mean active layer for active width (m)	Travel distance (m)	Volume (m^3)
January 2017–August 2017	58	0.24	440	4716
August 2017–December 2017	31	0.05	1037	1238
December 2017–September 2018	52	0.1	1002	4012
Total				9966 (5711)

References

Anderson, S.W., 2019. Uncertainty in quantitative analyses of topographic change: error propagation and the role of thresholding. Earth Surf. Process. Landf. 44 (5), 1015–1033.

Ashmore, P., 2013. Morphology and dynamics of braided rivers. In: Shroder, J.F., Wohl, E. (Eds.), Treatise on Geomorphology. Academic Press, Sans Diego CA, pp. 289–312.

Astrade, L., Jacob-Rousseau, N., Bravard, J.P., Allignol, F., Simac, L., 2011. Detailed chronology of mid-altitude fluvial system response to changing climate and societies at the end of the Little Ice Age (Southwestern Alps and Cévennes, France). Geomorphology 133, 100–116.

B.I.G, 1979. Etude de la nappe alluviale du Drac entre le confluent des Drac de Champoléon et d'Orcières, et le lac du Sautet (49 p).

Belletti, B., Dufour, S., Piegay, H., 2013. Regional variability of aquatic pattern in braided reaches (example of the French Rhône basin). Hydrobiologia 712, 25–41.

Bravard, J.P., Peiry, J.L., 1993. La disparition du tressage fluvial dans les Alpes françaises sous l'effet de l'aménagement des cours d'eau (19-20ème siècles). Zeitschrift für Geomorphologie, Supplement Band. 88, 67–79.

Bravard, J.P., Amoros, C., Pautou, G., Bornette, G., Bournaud, M., Creuzé Des Châtelliers, M., Gibert, J., Peiry, J.L., Perrin, J.F., Tachet, H., 1997. River incision in South-East France: morphological phenomena and ecological effects. Regul. Rivers Res. Manag. 13, 1–16.

Brousse, G., Arnaud-Fassetta, G., Liébault, F., Bertrand, M., Melun, G., Loire, R., Malavoi, J.R., Fantino, G., Borgniet, L., 2020. Channel response to sediment replenishment in a large gravel-bed river: the case of the Saint-Sauveur dam in the Buëch River (Southern Alps, France). River Res. Appl. 1, 14. https://doi.org/10.1002/rra.3527.

Brousse, G., Arnaud-Fassetta, G., Liébault, F., Vasquez-Tarrio, D., 2018. Experimental bed active layer survey with active RFID scour chains: example of two braided rivers in the French Alps (the Drac and the Vénéon). In: Paquier, A., Rivière, N. (Eds.), RiverFlow 2018. 40. E3S Web of Conferences, Lyon-Villeurbanne.

Bunte, K., 2004. Gravel Mitigation and Augmentation Below Hydroelectric Dams: A Geomorphological Perspective. Engineering Research Center, Fort Collins (144 p).

Bunte, K., Abt, S.R., 2001. Sampling surface and subsurface particle-size distributions in wadable gravel- and cobble-bed streams for analyses of sediment transport, hydraulics, and streambed monitoring. USDA Forest Service, Rocky Mountains Research Station, General Technical Report. 74 (428 p).

Caruso, B.S., 2006. Project river recovery: restoration of braided gravel-bed river habitat in New Zealand's high country. Environ. Manag. 37 (6), 840–861. https://doi.org/10.1007/s00267-005-3103-9.

Cassel, M., Piégay, H., Lavé, J., 2016. Effects of transport and insertion of radio frequency identification (RFID) transponders on resistance and shape of natural and synthetic pebbles: applications for riverine and coastal bedload tracking. Earth Surf. Process. Landf. 42, 399–413. https://doi.org/10.1002/esp.3989.

Cassel, M., Dépret, T., Piégay, H., 2017. Assessment of a new solution for tracking pebbles in rivers based on active RFID. Earth Surf. Process. Landf. 42, 1938–1951. https://doi.org/10.1002/esp.4152.

Cassel, M., Piégay, H., Fantino, G., Lejot, J., Bultingaire, L., Michel, K., Perret, F., 2020. Geopositioning error estimates for a-UHF artificial pebble tracers: comparison of ground-based and UAV surveys on a braided river. Earth Surf. Process. Landf. 45-5, 1123–1140. https://doi.org/10.1002/esp.4777.

Church, M., Jones, D., 1982. Channel bars in gravel-bed rivers. In: Hey, R.D., Bathurst, J.C., Thorne, C.R. (Eds.), Gravel-bed Rivers. John Wiley and Sons, Chichester, pp. 291–338.

CLEDA, 2010. Contrat de Rivière du Drac amont (74 p).

Comiti, F., Da Canal, M., Surian, N., Mao, L., Picco, L., Lenzi, M.A., 2011. Channel adjustments and vegetation cover dynamics in a large gravel bed river over the last 200 years. Geomorphology 125, 147–159.

Downs, P.W., Kondolf, G.M., 2002. Post-project appraisals in adaptive management of river channel restoration. Environ. Manag. 29, 477–496. https://doi.org/10.1007/s00267-001-0035-X.

ETRM, 2010. Plan de gestion et d'entretien du lit du Drac et de ses principaux affluents. Quantification du transport solide (70 p).

Habersack, H., Piégay, H., 2007. River restoration in the Alps and their surroundings: past experience and future challenges. In: Rinaldi, M., Habersack, H., Piégay, H. (Eds.), Gravel-bed Rivers VI: From Process Understanding to River Restoration. Elsevier Science, Amsterdam, pp. 703–737.

Haschenburger, J., Church, M., 1998. Bed material transport estimated from the virtual velocity of sediment. Earth Surf. Process. Landf. 23, 791–808.

Hicks, D.M., Shankar, U., Duncan, M.J., Rebuffé, M., Aberle, J., 2009. Use of remote-sensing technology to assess impacts of hydro-operations on a large, braided, gravel-bed river: Waitaki River, New Zealand. In: Sambrook Smith, G.H., Best, J.L., Bristow, C.S., Petts, G.E., Jarvis, I. (Eds.), Braided Rivers: Process, Deposits, Ecology and Management. John Wiley and Sons, Chichester, pp. 311–326.

Ioana-Toroimac, G., Zaharia, L., Minea, G., Moroşanu, G.G., 2017. Using a multi-criteria analysis to identify rivers with hydromorphological restoration priority: braided rivers in the south-eastern Subcarpathians (Romania). Sci. Total Environ. 599-600, 700–709. https://doi.org/10.1016/j.scitotenv.2017.04.209.

Kondolf, G.M., Gao, Y., Annandale, G.W., Morris, G.L., Jiang, E., Zhang, J., Cao, Y., Carling, P., Fu, K., Guo, Q., Hotchkiss, R., Peteuil, C., Sumi, T., Wang, H.W., Wang, Z., Wei, Z., Wu, B., Wu, C., Yang, C.T., 2014. Sustainable sediment management in reservoirs and regulated rivers: experiences from five continents. Earth's Future 2 (5), 256–280.

Lallias-Tacon, S., 2015. Analyse spatio-temporelle de la morphologie des rivières en tresses par LiDAR aéroporté. Thèse de doctorat. 2. Université Lyon (213 p).

Lallias-Tacon, S., Liébault, F., Piégay, H., 2014. Step by step error assessment in braided river sediment budget using airborne LiDAR data. Geomorphology 214, 307–323.

Lallias-Tacon, S., Liebault, F., Piégay, H., 2017. Use of airborne LiDAR and historical aerial photos for characterising the history of braided river floodplain morphology and vegetation responses. Catena 149, 742–759.

Laval, F., Guilmin, E., 2014. Upper Drac River restoration project: restoration of a braided river bed incised in clay substratum through sediment reloading and bed widening. SHF Conference. BURGEAP, Nantes.

Le Lay, Y.F., Piégay, H., Rivière-Honegger, A., 2013. Perception of braided river landscapes: implications for public participation and sustainable management. J. Environ. Manag. 119, 1–12. https://doi.org/10.1016/j.jenvman.2013.01.006.

Leclair, R., 2016. Pressions anthropiques et ajustements hydromorphologiques dans le bassin-versant de l'Isère du XVIII^{e} siècle à 1950. Mémoire de master 2. Université Paris-Diderot (188 p).

Liébault, F., Laronne, J.B., 2008. Evaluation of bedload yield in gravel-bed rivers using scour chains and painted tracers: the case of the Esconavette Torrent (Southern French Prealps). Geodin. Acta 21, 23–34. https://doi.org/10.3166/ga.21.23-34.

Liébault, F., Piégay, H., 2002. Causes of 20th century channel narrowing in mountain and piedmont rivers of Southeastern France. Earth Surf. Process. Landf. 27, 425–444.

Liébault, F., Gomez, B., Page, M., Marden, M., Peacock, D., Richard, D., Trotter, C.M., 2005. Land-use change, sediment production and channel response in upland regions. River Res. Appl. 21 (7), 739–756.

Liébault, F., Lallias-Tacon, S., Cassel, M., Talaska, N., 2013. Long profile responses of alpine braided rivers in SE France. River Res. Appl. 29, 1253–1266. https://doi.org/10.1002/rra.2615.

Mao, L., Picco, L., Lenzi, M.A., Surian, N., 2017. Bed material transport estimate in large gravel-bed rivers using the virtual velocity approach. Earth Surf. Process. Landf. 42 (4), 595–611.

Marmonier, P., Olivier, M.J., Creuzé des Châtelliers, M., Paran, F., Graillot, D., Winiarski, T., Konecny-Dupré, L., Navel, S., Cadilhac, L., 2019. Does spatial heterogeneity of hyporheic fauna vary similarly with natural and artificial changes in braided river width? Sci. Total Environ. 689, 57–69. https://doi.org/10.1016/j.scitotenv.2019.06.352.

Misset, C., 2019. The Role of Riverbed on Suspended Sediment Transport Dynamics in Alpine Catchments. Thèse de doctorat. Université Grenoble Alpes (243 p).

Montjuvent, G., 1978. Le Drac: morphologie, stratigraphie et chronologie quaternaires d'un bassin alpin. Thèse de doctorat. Université de Grenoble II (421 p).

Muhar, S., Seliger, C., Schinegger, R., Scheikl, S., Brändle, J., Hayes, D.S., Schmutz, S., 2019. Status and protection of rivers: A pan-alpine overview. In: Muhar, S., Muhar, A., Egger, G., Siegrist, D. (Eds.), Rivers of the Alps, Diversity in Nature and Culture. Haupt, Berne, pp. 302–319.

Nanson, G., Knighton, D., 1996. Anabranching rivers: their cause, character and classification. Earth Surf. Process. Landf. 21 (3), 217–239.

Piégay, H., Grant, G., Nakamura, F., Trustrum, N., 2006. Braided river management: from assessment of river behavior to improved sustainable development. In: Sambrook Smith, G.H., Best, J.L., Bristow, C.S., Petts, G.E. (Eds.), Braided Rivers: Process, Deposits, Ecology and Management. Blackwell, Oxford, pp. 257–274.

Piégay, H., Alber, A., Slater, L., Bourdin, L., 2009. Census and typology of braided rivers in the French Alps. Aquat. Sci. 71, 371–388.

Recking, A., 2009. Theoretical development on the effects of changing flow hydraulics on incipient bed load motion. Water Resour. Res. 45 (4), 1–16. https://doi.org/10.1029/2008WR006826.

Recking, A., 2013a. A simple method for calculating reach-averaged bedload transport. J. Hydraul. Eng. 139, 70–75. https://doi.org/10.1061/(ASCE)HY.1943-7900.0000653.

Recking, A., 2013b. An analysis of nonlinearity effects on bed load transport prediction. Journal of Geophysical Research-Earth Surface 118, 1264–1281. https://doi.org/10.1002/jgrf.20090.

Roni, P., Liermann, M., Muhar, S., Schmutz, S., 2013. Monitoring and evaluation of restoration actions. In: Roni, P., Beechie, T. (Eds.), Stream and Watershed Restoration: A Guide to Restoring Riverine Processes and Habitats. John Wiley & Sons, Chichester, pp. 254–279.

Roux, C., Alber, A., Bertrand, M., Vaudor, L., Piégay, H., 2015. "FluvialCorridor": a new ArcGIS toolbox package for multiscale riverscape exploration. Geomorphology 242, 29–37.
Schumm, S.A., 1981. Evolution and response to the fluvial system, sedimentologic implications. In: Ethridge, F.G., Flores, R.M. (Eds.), Recent and Ancient Nonmarine Environments: Models for Exploration. SEPM, Special Publication 31, pp. 19–29.
Staentzel, C., Kondolf, M., Schmitt, L., Combroux, I., Barillier, A., Beisel, J.N., 2020. Restoring fluvial forms and processes by gravel augmentation or bank erosion below dams: a systematic review of ecological responses. Sci. Total Environ. 706, 135743.
Sumi, T., 2006. Reservoir sediment management measures and necessary instrumentation technologies to support them. The 6th Japan-Taiwan Joint Seminar on Natural Hazard Mitigation, Kyoto.
Surian, N., Cisotto, A., 2007. Channel adjustments, bedload transport and sediment sources in a gravel-bed river, Brenta River, Italy. Earth Surf. Process. Landf. 32, 1641–1656.
Surian, N., Rinaldi, M., 2003. Morphological response to river engineering and management in alluvial channels in Italy. Geomorphology 50, 307–326.
Terrier, B., Piégay, H., Lébault, F., Dufour, S., Belleti, B., Le Lay, Y.F., Marmonier, P., Comby, E., Tacon, S., Faton, J.M., Gourhand, A., Marteau, B., Râpple, B., Wawrzyniak, V., 2019. Les rivières en tresses - Elements de connaissances. Guide Technique, Bassin Rhône Méditerranéen (116 p).
Vivian, H., Thomas, A., 1982. Erosion et transports solides dans le bassin du Haut Drac (en amont de la retenue du Sautet). Unpublished technical report. Cemagref, Division Protection contre les Erosions, Grenoble (105 p).
Ward, J.V., Tockner, K., Edwards, P.J., Kollmann, J., Bretschko, G., Gurnell, A.M., Petts, G.E., Rossaro, B., 1999. A reference river system for the Alps: the "Fiume Tagliamento". Regul. Rivers Res. Manag. 15, 63–75.
Wolman, G., 1954. A method of sampling coarse river-bed material. Trans. Am. Geophys. Union 35 (6), 951–956.
Wyzga, B., Zawiejska, J., Hajdukiewicz, H., 2016. Multi-thread rivers in the Polish Carpathians: occurrence, decline and possibilities of restoration. Quat. Int. 415, 344–356.